

Development of Substrate-Independent Antifouling and Bactericidal Surfaces Using Visible Light Cross-Linked Hydrogel Coatings for Biomedical Applications

Soonjong Roh, Se Youn Jang, Youngmee Jung, Kangwon Lee,* and Jin Yoo*

Preventing biofouling and bacterial infections are pivotal issues in developing implantable biomaterials. Zwitterionic hydrogels stand out for their antifouling effects and high biocompatibility, making them ideal for biomedical applications. However, the lack of direct bactericidal activity and the limited applicability to various materials are key challenges to be addressed in these hydrogel coatings. To address this, a dual-functional hydrogel coating with synergetic antifouling and biocidal properties is proposed to prevent the initial infection and consequent biofilm formation, which can be applied to various types of substrates. This coating is fabricated via photo-crosslinking, combining representative zwitterionic polymer, poly (sulfobetaine methacrylate) (pSBMA), with a cationic bactericidal polymer, poly (2-aminoethyl methacrylate) (pAEMA). Owing to antifouling and contact-killing properties, the p(SBMA-co-AEMA) hydrogel-coated surface can repel non-specific proteins and eradicate bacteria such as *E. coli* and *S. aureus* that overcame the antifouling barrier. These results also demonstrate that this hydrogel coating exhibits excellent biocompatibility and can be applied to various substrate materials from polymers to metals. The coating method developed in this study holds great potential for enhancing the performance and safety of various implantable biomaterials and medical devices.

millions of individuals.^[1] On the other hand, preventing implant-associated infections has emerged as a significant challenge in developing these medical devices (e.g., stents, catheters, and pacemakers). Such infections can trigger diverse foreign body reactions (FBRs) and compromise the functionality of medical devices, impeding the delivery of appropriate clinical interventions.^[2,3] Conventional implant biomaterials, encompassing metals, polymers, and ceramics, often lack inherent self-cleaning capabilities.^[4] Consequently, extensive research efforts have been devoted to surface modification strategies to overcome this limitation.^[3,5-9]

Investigating and preventing biofouling is necessary, as it begins with the adsorption of minute organic particles, such as proteins, onto surfaces.^[10] This process, in turn, facilitates bacterial colonization and biofilm formation.^[1] To address these issues, hydrogel coatings are increasingly recognized for their exceptional antifouling efficacy and high biocompatibility.^[1,11] Designed to prevent

the adhesion of non-specific proteins, these coatings form a thick hydration layer on surfaces, creating steric hindrance and an energetic barrier against fouling.^[12] Moreover, their high grafting

1. Introduction

Over the past few decades, implantable medical devices have significantly advanced life quality and prolonged lifespans for

S. Roh, S. Y. Jang, Y. Jung, J. Yoo
Biomaterials Research Center
Korea Institute of Science and Technology (KIST)
Seoul 02792, Republic of Korea
E-mail: jyoo@kist.re.kr

S. Roh, K. Lee
Department of Applied Bioengineering
Graduate School of Convergence Science and Technology
Seoul National University
Seoul 08826, Republic of Korea
E-mail: kangwonlee@snu.ac.kr

 The ORCID identification number(s) for the author(s) of this article can be found under <https://doi.org/10.1002/adhm.202402565>

© 2025 The Author(s). Advanced Healthcare Materials published by Wiley-VCH GmbH. This is an open access article under the terms of the [Creative Commons Attribution-NonCommercial-NoDerivs License](#), which permits use and distribution in any medium, provided the original work is properly cited, the use is non-commercial and no modifications or adaptations are made.

DOI: 10.1002/adhm.202402565

S. Y. Jang
KU-KIST Graduate School of Converging Science and Technology
Korea University
Seoul 02841, Republic of Korea

Y. Jung
School of Electrical and Electronic Engineering
YU-KIST Institute
Yonsei University
Seoul 03722, Republic of Korea

K. Lee
Research Institute for Convergence Science
Seoul National University
Gyeonggi-do 16229, Republic of Korea

Y. Jung, J. Yoo
Division of Bio-Medical Science and Technology
KIST School
Korea University of Science and Technology (UST)
Seoul 02792, Republic of Korea

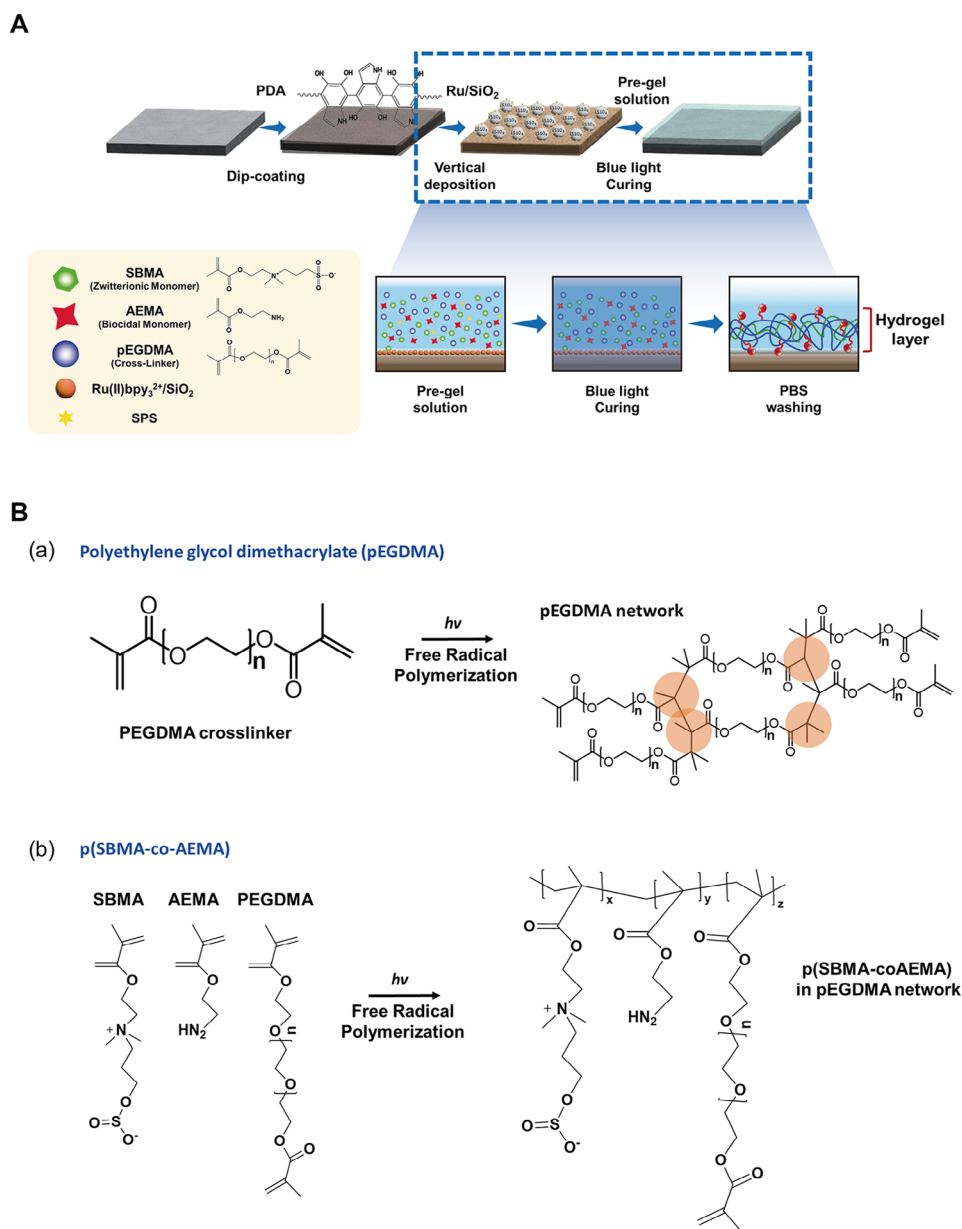


Figure 1. Design of versatile dual-functional p(SBMA-co-AEMA) hydrogel coating.

density, uniform coverage, and ability to precisely control thickness give hydrogel coatings significant advantages over polymer brushes.^[13]

Recently, polyzwitterionic polymers have been widely used as substitutes for poly(ethylene glycol) (PEG) due to their enhanced coating stability and superior antifouling properties.^[14,15] Additionally, several researchers have reported poly(ylides) as a new class of unexplored zwitterionic materials. Notable advancements in antifouling research include the exploration of N-oxide-based materials,^[16,17] sulfur ylides, and phosphorous ylides.^[18,19] Despite these developments, zwitterionic groups, such as poly(sulfobetaine methacrylate) (pSBMA), remain a popular choice due to their biocompatibility and effective antifouling properties. These materials uniformly distribute both negative and positive

charges within their structure, allowing more water molecules to be retained in the hydration layer and increasing resistance to dehydration.^[20] Furthermore, the ionic strength resistance of the zwitterionic moieties stabilizes the modified surface under varying ionic and oxidative conditions.^[21] However, several challenges remain, including limitations on the types of coating substrates, the use of toxic solvents to anchor the initiators, and the inability to eliminate bacteria that have already adhered. Therefore, developing a universal coating method applicable to any surface (e.g., metals, polymers, and ceramics) and eradicating bacteria that overcome the anti-adhesion barrier becomes major challenges in antifouling hydrogel coatings.^[22]

Bactericidal surfaces can be achieved by releasing bactericidal agents or directly killing bacteria on the surface

(contact-killing). While release-based bactericidal surfaces are highly effective, they face limitations such as the finite longevity of the agents, challenges in controlling release rates, and the potential for resistance development with prolonged exposure. In contrast, contact-killing surfaces maintain a long-lasting antibacterial effect as long as the surface remains intact.^[22] They work primarily by disrupting the membranes of adhering bacteria through cationic agents including various amine-containing polymers, chitosan, and antimicrobial peptides (AMPs).^[12] These surfaces can benefit from the selective toxicity of the amine groups, especially targeting the more negatively charged bacterial cell membranes over eukaryotic cells due to their differences in membrane composition and structure.^[23]

To fully meet the desired requirements, this study introduces a substrate-independent hydrogel coating technique that combines the antifouling characteristics of a polyzwitterionic polymer with the bactericidal properties of a primary amine-based polymer, utilizing visible light cross-linking. To immobilize the photoinitiator-loaded SiO₂ nanoparticles (NPs) onto the substrate, we dip-coated the target surfaces with a polydopamine (pDA) layer, which facilitated strong adhesion of the NPs to the substrate. Unlike previously reported hydrogel coating methods that use benzophenone,^[24,25] which are limited to polymeric surfaces, the use of pDA expands the applicability to a broader range of substrates. The antifouling functionality was achieved by synthesizing zwitterionic pSBMA hydrogel on the surfaces through photo-crosslinking. Notably, the physical properties of the hydrogel, as well as its antifouling and antithrombogenic performance, were optimized at a specific concentration of the cross-linker, poly(ethylene glycol dimethacrylate) (pEGDMA). Moreover, the addition of bactericidal poly(2-aminoethyl methacrylate) (pAEMA) not only effectively prevented biofilm formation but also strengthened the adhesive interactions between the surfaces and the hydrogel layer through Michael addition or Schiff base reactions, thereby forming strong bonds.^[26,27] Conclusively, the novelty of this study lies in its universally applicable coating process under extremely mild conditions and the dual functionality of the antifouling and bactericidal p(SBMA-co-AEMA) hydrogel with enhanced physical stabilities. Based on this coating method, vulnerable and sensitive biomaterials can now be explored for use in implantable biomedical devices without the risk associated with toxic organic solvents and bacterial infections.

2. Results and Discussion

2.1. Fabrication of Zwitterionic pSBMA Hydrogel Coating

Figure 1A delineates the scheme of the zwitterionic hydrogel coating, comprising three pivotal steps. Initially, pDA was employed to confer adhesive properties on the hydrogel layer across diverse substrate types. Subsequently, a suspension of SiO₂ NPs adsorbed with Ru(bpy)₃ was applied onto the pDA-coated substrates to anchor the photoinitiator on the surface. These SiO₂ NPs play an instrumental role in evenly distributing the photoinitiator and enhancing its photochemical reactivity through electrostatic bonding with Ru(bpy)₃ as a non-covalent interaction, thereby improving the coating stability (**Figure S1**, Supporting Information).^[28] The hydrogel layer was then formed by immers-

Table 1. Summary of compositions for fabricating different hydrogel coatings.

Sample	SBMA [g]	AEMA [mg]	pEGDMA [g]	1X PBS [mL]
SHG0.1 ^{a)}	2	–	0.1	10
SHG0.3	2	–	0.3	10
SHG0.5	2	–	0.5	10
SAHG0.5 ^{b)}	2	80	0.5	10

^{a)} SHG denotes pSBMA hydrogel; ^{b)} SAHG denotes p(SBMA-co-AEMA) hydrogel.

ing the substrates in the pre-gel solutions and curing them under blue light for 3 min.

The pre-gel solution consisted of monomers, a cross-linker, and sodium persulfate (SPS). When exposed to visible light, the photo-excited Ru²⁺ oxidizes into Ru³⁺ by transferring electrons to SPS. Upon receiving the electrons, SPS dissociates into sulfate anions and sulfate radicals. These radicals then initiate the cross-linking of pSBMA by propagating through the methacryloyl groups (**Figure 1B**).^[29] To optimize hydrogel formation, pre-gel solutions were prepared with different concentrations of pEGDMA, specifically 0.1, 0.3, and 0.5 g in 10 mL of PBS. The final zwitterionic hydrogel condition was determined by evaluating each hydrogel through physicochemical analysis and antifouling tests, as detailed in the three experimental groups shown in **Table 1**.

2.2. Surface Characterization of Zwitterionic pSBMA Hydrogel

The surface morphologies of zwitterionic pSBMA hydrogels (SHG) with varying concentrations of the cross-linker pEGDMA were analyzed using scanning electron microscopy (SEM), as shown in **Figure 2A**. First, pDA aggregates and SiO₂ NPs were sequentially observed on the Si wafer following each pre-coating step, contrasting with the pristine Si wafer. After the hydrogel coating, relatively flat top surfaces and porous structures appeared in SHG0.3 and SHG0.5, indicating successful hydrogel layer formation in these groups, except for SHG0.1. Interestingly, as the pEGDMA concentration increased, SHG0.5 exhibited more uniform and circular pores, whereas SHG0.3 had irregular and elongated shapes in the cross-sectional images (insets in the SEM images). Furthermore, surface roughness, as analyzed by atomic force microscopy (AFM), showed that higher pEGDMA concentrations led to smoother surfaces, as seen in SHG0.5, due to tighter cross-linking (**Figure 2B**).

The chemical composition of the zwitterionic hydrogel was confirmed by Fourier transform infrared (FTIR) spectroscopy (**Figure 2C**). The FTIR spectra of each layer demonstrated successful deposition following each coating step. The bands at 800 cm⁻¹ (Si–O bending) and 957 cm⁻¹ (Si–OH stretching) indicated the deposited SiO₂ NPs on the pDA-coated layer. After hydrogel coating, the hydration layer was signified by 3550–3200 cm⁻¹ range from the hydroxyl group (O–H stretching) and a band of 1715 cm⁻¹, demonstrating the formation of hydrogel layer from its carbonyl group (C=O stretching).^[30] The bands at 1644 cm⁻¹ (C–N stretching) and 1480 cm⁻¹ were observed in SHG0.3 and SHG0.5, derived from the quaternary ammonium of pSBMA (C–N). Moreover, the vibration peak at 1029 cm⁻¹

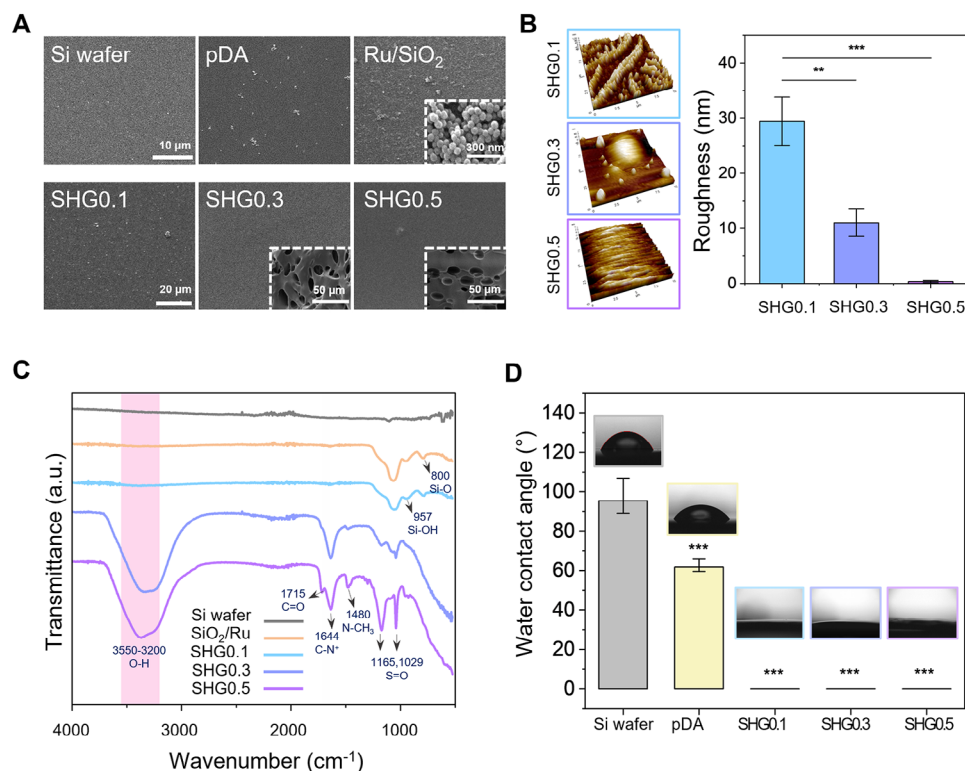


Figure 2. Characterization of zwitterionic SHG coatings. A) Surface morphology of SHG coating with different ratios of cross-linker observed by SEM images. Insets in the SEM images provide a closer view (upper row) and cross-sectional images (lower row), respectively. B) Surface roughness of SHG0.1, SHG0.3, and SHG0.5 coating. $***p < 0.001$ and $**p < 0.01$. C) ATR-FTIR spectra and D) water contact angles for each step in SHG coating process. $***p < 0.001$ compared to the pristine Si wafer.

(S=O) and 1165 cm^{-1} (S=O) also proved the formation of pSBMA.^[24]

The antifouling properties of hydrogel coatings are attributed to their high surface energy, which creates thermodynamically unfavorable conditions that prevent the non-specific adsorption of proteins.^[1,31] The water contact angle (WCA) was measured to evaluate each coating layer's surface energy (Figure 2D). Due to the hydrophilicity of pDA, the WCA slightly decreased from $95.5 \pm 9.8^\circ$ for the pristine Si wafer to $61.8 \pm 3.7^\circ$ for the pDA-coated surface. The WCA drastically reduced to 0° across all hydrogel-coated groups, regardless of the pEGDMA concentration. Despite previous results indicating that SHG0.1 did not form a hydrogel layer on surfaces, the presence of deposited SiO_2 NPs seemed to impact the WCA, likely due to the polar silanol groups^[32] and residual pSBMA on the SHG0.1 surface (Figure S2, Supporting Information). These findings confirm that pSBMA contributes to the superhydrophilic properties of coatings.

2.3. Mechanical Properties and Biocompatibility of Zwitterionic pSBMA Hydrogel

In dynamic environments where body fluids are present, the mechanical strength of a coating layer is crucial. This is because deformation of the coating under fluidic conditions can lead to device malfunction and potentially exacerbate infections.^[20] To

evaluate the mechanical properties of each hydrogel, rheological property and swelling behavior were analyzed. SHG0.5 exhibited the highest storage modulus (G') across all frequencies compared to the other groups, indicating superior stability of the pSBMA hydrogel under shear stress (Figure 3A). Since SHG0.1 demonstrated liquid-like characteristics, with storage modulus values similar to those of the loss modulus (G''), swelling ratio comparisons were only conducted between SHG0.3 and SHG0.5. Generally, zwitterionic hydrogels exhibit a high swelling ratio due to their strong affinity for water molecules, which raises concerns about detachment from the coating surface because of the discrepancy in mechanical strength between the coated hydrogel and the substrate.^[33] As illustrated in Figure 3B, SHG0.5 exhibited a lower swelling ratio compared to SHG0.3, reaching equilibrium just after day 1. This outcome suggests that pEGDMA enhances the coating stability by creating a denser hydrogel network, which restricts the swelling of pSBMA chains by water molecules.^[34]

To ensure the biocompatibility of the coatings on mammalian cells, the cytotoxicity of the SHG coating layer was assessed using human dermal fibroblasts (HDFs). HDFs were cultured for 24 h in the extraction medium from an SHG-coated silicon wafer, followed by live/dead staining and cell viability assay (Figure 3C). The results showed that all groups with the SHG coating maintained cell viability above 80%, confirming that SHG is sufficiently biocompatible for biomedical applications.

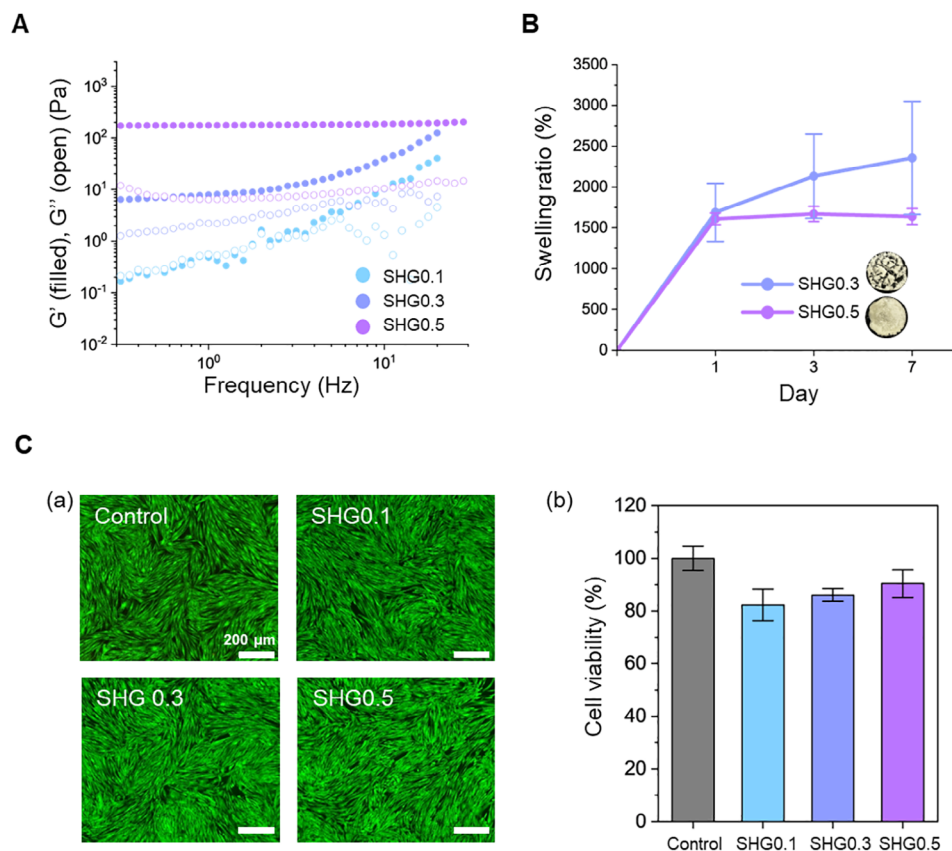


Figure 3. Mechanical properties and biocompatibility of zwitterionic SHG coatings. A) Oscillatory shear rheological properties of SHG0.1, SHG0.3 and SHG0.5. The filled and open points represent the storage modulus (G') and the loss modulus (G''), respectively. B) Swelling behaviors of SHG0.3 and SHG0.5 for 7 days. C) (a) Live/dead staining of HDFs cultured with or without SHG (Green: live cells, Red: dead cells) and (b) Quantification of cell viability using CCK-8 assay after 24 h.

2.4. Antifouling Performance and Applicability of Zwitterionic pSBMA Hydrogel

The antifouling properties of the SHG-coated surfaces were evaluated by their resistance to the adsorption of cells, platelets, and proteins. First, cell adhesion was examined by culturing HDFs on the pristine and SHG-coated surfaces for 24 h (Figure 4A). The results revealed that antifouling effects varied with the concentrations of the cross-linker. Only a few immature, round-shaped HDFs were observed on the SHG0.3 and SHG0.5 surfaces, whereas the pristine Si wafer and SHG0.1 surfaces had dense and fully stretched cells. Particularly, the SHG0.5 coating significantly reduced cell adhesion rates compared to the pristine substrate, indicating that a high concentration of cross-linker positively impacts antifouling effects. Cell adhesion may be disrupted for two major reasons related to zwitterionic moieties. First, the formation of a robust hydration shell makes it thermodynamically unfavorable for cells to penetrate, as the alternating positive and negative moieties strongly interact with water molecules. Additionally, the incorporation of the pEGDMA enhances water retention, helping the hydrogel maintain its conformation and providing greater resistance to biomolecules. The second reason is steric hindrance of zwitterionic polymer chains. These chains tend to return to their original swelling state, due

to their hydrophilic nature, after being deformed by foulants. This resilience prevents cells from attaching to the zwitterionic hydrogel-coated surface.^[35,36] Furthermore, the inhibitory effect of SHG0.5 on platelet activation was observed from the SEM images (Figure 4B). This confirmed that the coating conditions of SHG0.5 effectively contribute to its antifouling capabilities, considering that platelet activation is influenced by surface stiffness and topography.^[37,38]

Subsequently, protein resistance was evaluated by QCM-D, which monitored in situ protein adsorption on the surface. The frequency shifts indicated the amounts of adsorbed bovine serum albumin (BSA) and human fibrinogen (hFg) on the pristine gold quartz and SHG0.5-coated surfaces (Figure 4C), where a decreasing frequency indicates increasing protein adsorption on the surface.^[10] The frequency values of the SHG0.5-coated surface remained unchanged in both protein solutions of BSA and hFg. In contrast, those of the pristine quartz surface drastically dropped, demonstrating the dramatic antifouling efficacy of the SHG0.5 coating. This result indicates that an intact hydrogel layer was formed on the surface of the gold quartz, preventing non-specific adsorption, consistent with the results of cell and platelet adhesion.

Figure 4D shows SHG0.5 coated on various materials including PET, PS, PTFE, Cu, SUS (Stainless steel), Al, and

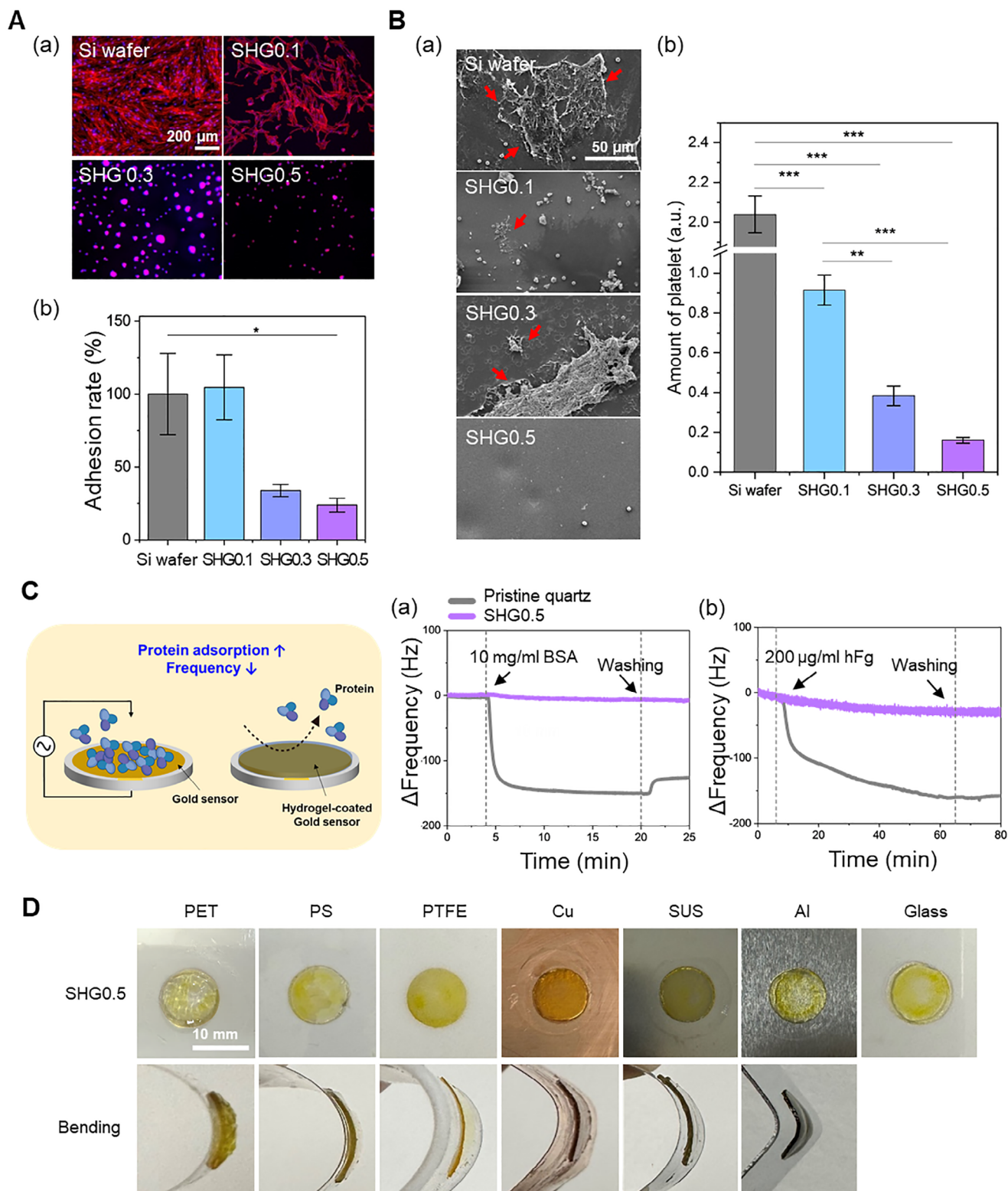


Figure 4. Antifouling and applicability of SHG coating. A) Cell morphology by Alexa Fluor 594-Phalloidin/DAPI staining (Red: F-actin, Blue: Nuclei) and adhesion rate of HDFs on pristine Si wafer and SHG-coated surfaces. $*p < 0.005$. B) SEM images of platelets adhered to pristine Si wafer and SHG-coated surfaces, along with the quantification of platelet activation on pristine and SHG-coated Si-wafers. $**p < 0.01$ and $***p < 0.001$. C) QCM-D measurements of BSA and hFg on pristine and SHG0.5-coated surfaces. D) Digital images of the SHG0.5 coating on various substrates.

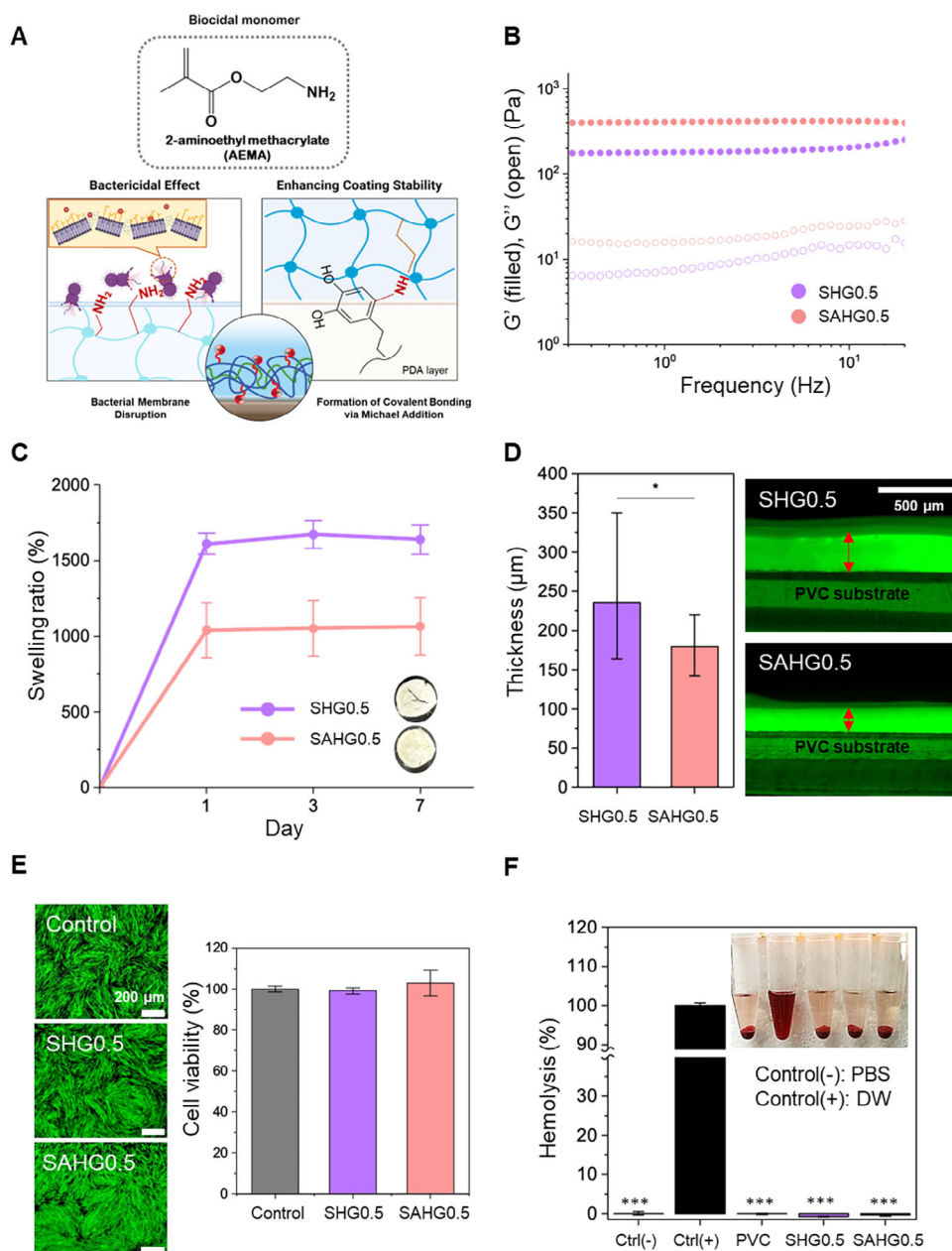


Figure 5. Introduction of AEMA and characterization of SAHG0.5. A) Schematic illustrations of AEMA B) Comparison of rheological properties between SHG0.5 and SAHG0.5. The filled and open points represent the storage modulus (G') and the loss modulus (G''), respectively. C) Swelling behaviors of SHG0.5 and SAHG0.5 for 7 days. D) Fluorescent images and thickness measurement of SHG0.5 and SAHG0.5 coating layers. E) Live/dead staining of HDFs cultured with SHG0.5 and SAHG0.5. (Green: live cells, Red: dead cells) and quantification of cell viability using CCK-8 assay after 24 h. F) Hemolysis rates of SHG0.5 and SAHG0.5. *** $p < 0.001$ compared to Ctrl(+).

glass. Owing to the versatile adhesive properties of pDA^[39,40] and photo-crosslinking with visible light, all the substrates displayed the desired circular coating layer on their surfaces. Even when the substrate was bent, the coating layer remained intact without peeling, demonstrating the applicability of SHG0.5 to both metallic and polymeric biomaterials. Consequently, we focused on the SHG0.5 coating in the subsequent bactericidal studies.

2.5. Introduction of Amine-Containing Monomer to Fabricate Bactericidal Hydrogel

As depicted in **Figure 5A**, the bactericidal surface was achieved by adding AEMA to the optimized zwitterionic hydrogel (SHG0.5). Primary amines are known for their superior bactericidal activity and high selectivity. Positively charged primary amines can easily disrupt the outer membranes of bacteria with a negative

charge.^[41] Additionally, their amino group (-NH₂) can easily participate in reactions with electrophiles. This reactivity enables primary amines to exhibit synergistic effects, either by combining with other antimicrobial agents or by enhancing adhesive strength when used with surfaces modified by pDA.^[42]

The concentration of AEMA was optimized considering both bactericidal effect and low cytotoxicity (Figure S3, Supporting Information). To confirm the formation of p(SBMA-co-AEMA) (SAHG0.5) coating on polyvinyl chloride (PVC) which is one of the common medical polymers, the chemical composition was analyzed by SEM/EDS, FTIR, and XPS (Figure S4, Supporting Information). The mechanical properties of SAHG0.5 were analyzed by a rheological variation, swelling ratio, and thickness measurement.

In the rheological analysis, SAHG0.5 also showed a gel property ($G' > G''$) but was stiffer than SHG0.5 with a slightly increased G' value (Figure 5B). The storage modulus of the SAHG0.5 was similar to that of human soft tissue, which might enhance the coating durability by preventing damage from the dynamic environment in the human body.^[43] Furthermore, the 33% reduction in the swelling ratio of SAHG0.5, achieved through the addition of AEMA, demonstrated enhanced mechanical strength (Figure 5C, Figure S5, Supporting Information). A lower swelling property can help maintain adhesion considering that the swelling forces exceeding the strength of the hydrogel network lead to hydrogel detachment.^[44] The thickness of the SHG0.5 and SAHG0.5 coating layers was visualized under wet conditions using fluorescence microscopy (Figure 5D). Notably, SAHG0.5 exhibited a significantly reduced thickness ($179 \pm 32 \mu\text{m}$) compared to SHG0.5 ($236 \pm 69 \mu\text{m}$). A thinner hydrogel layer provides enhanced flexibility and improved conformity to the substrate surface, thereby strengthening interfacial adhesion and mechanical integrity without compromising the physical or functional properties of the hydrogel (Figures S6–S8, Supporting Information).^[45]

To verify biocompatibility after the introduction of a bactericidal substance like AEMA, in vitro cytotoxicity and hemolysis assays were conducted. Following the previous test method, HDFs were treated with the extraction of SAHG0.5 and cultured for 24 h. As depicted in Figure 5E, the cytotoxicity of SAHG0.5 did not significantly differ from the control and SHG0.5, exhibiting $\approx 100\%$ cell viability. Moreover, SHG0.5 and SAHG0.5-coated surfaces displayed low hemolysis rates comparable to that of negative control, implying that p(SBMA-co-AEMA) coating is harmless (Figure 5F).

2.6. Antifouling Performance of Dual-Functional p(SBMA-co-AEMA) Hydrogel

One of the primary concerns regarding dual-functional coatings is that antifouling and bactericidal activities may interfere with each other.^[22] Therefore, it is imperative to identify coating conditions that can effectively harmonize both functionalities. We first conducted an anti-cell adhesion test to determine the comparable antifouling effects of SAHG0.5 with zwitterionic SHG0.5 coating. As before, HDFs were directly seeded onto the pristine PVC and SAHG0.5-coated PVC, and observations were made on each day 1 and 3. Figure 6A shows fewer cells attached to the

SAHG0.5-coated surface than to the pristine PVC, which was covered with fully extended cells on day 1. Notably, there was no observed increase in cell adhesion and spreading even by day 3, suggesting that the SAHG0.5 coating maintains its inhibitory effect on cell attachment over time. Specifically, the cell adhesion rate showed a 66% and 73% decrease on the SAHG0.5-coated surface compared to the pristine PVC on days 1 and 3, respectively.

Blood-contacting devices should inhibit thrombus formation and platelet activation to maintain functionality without inducing inflammation. Generally, blood coagulation is initiated by the tissue factor (TF) protein and platelet activities, ultimately leading to the formation of a thrombus.^[46] To evaluate the antithrombogenicity of SAHG0.5, we exposed both pristine PVC and SAHG0.5-coated PVC to calcified whole blood and observed thrombus formation. Severe blood clots were detected on the pristine PVC, whereas the SAHG0.5-coated PVC exhibited a clean and transparent surface without thrombus formation (Figure 6B; Figure S9, Supporting Information). The amount of thrombus was quantified by detaching it from the surfaces and measuring the absorbance at 595 nm. The results showed that the absorbance of the SAHG0.5-coated PVC (0.04 ± 0.001) was seven times lower than that of the pristine PVC (0.12 ± 0.06). Moreover, when exposed to dynamic blood flow at a flow rate of 170 mL min^{-1} no blood clots were observed on the SAHG0.5-coated surface while a significant amount of clotting occurred on the pristine PVC over time (Figure S10, Supporting Information). The finding indicates that even in dynamic conditions, the anticoagulant properties of the SAHG0.5 coating are maintained without degradation. Platelet activation was analyzed by incubating each substrate (pristine PVC and SAHG0.5-coated PVC) in platelet-rich plasma (PRP) and determining the activity of lactate dehydrogenase (LDH), which increases with platelet activation. The colorimetric value of LDH significantly decreased in SAHG0.5-coated PVC (0.25 ± 0.05) compared to the pristine PVC (1.64 ± 0.19) (Figure 6C).

2.7. Bactericidal Performance of Dual-Functional p(SBMA-co-AEMA) Hydrogel

To assess the bactericidal properties of SAHG0.5, namely p(SBMA-co-AEMA), we examined bacterial attachment and biofilm formation using *Escherichia coli* (*E. coli*) and *Staphylococcus aureus* (*S. aureus*) as representative gram-negative and positive bacteria, respectively. Each bacteria solution was dropped on the pristine PVC, SHG0.5, and SAHG0.5 surfaces and incubated for 3 h. Bacterial presence on the surfaces was analyzed using live/dead staining, and the number of detached bacteria was determined through colony counting (Figure 7A). Numerous bacteria were observed on the pristine PVC surface, whereas only a few adhered to the SHG0.5 and SAHG0.5 surfaces. Notably, dead bacteria were found exclusively on the SAHG0.5 surface, indicating its contact-killing effect. Additionally, it was observed that bacteria detached from the SAHG0.5 surface were unable to form colonies both in *E. coli* and *S. aureus*, further demonstrating its bactericidal efficacy. While there was no significant difference in the number of detached *E. coli* between pristine PVC and SHG0.5, the SHG0.5 surface may promote bacterial growth by encapsulating surviving bacteria within the matrix. In con-

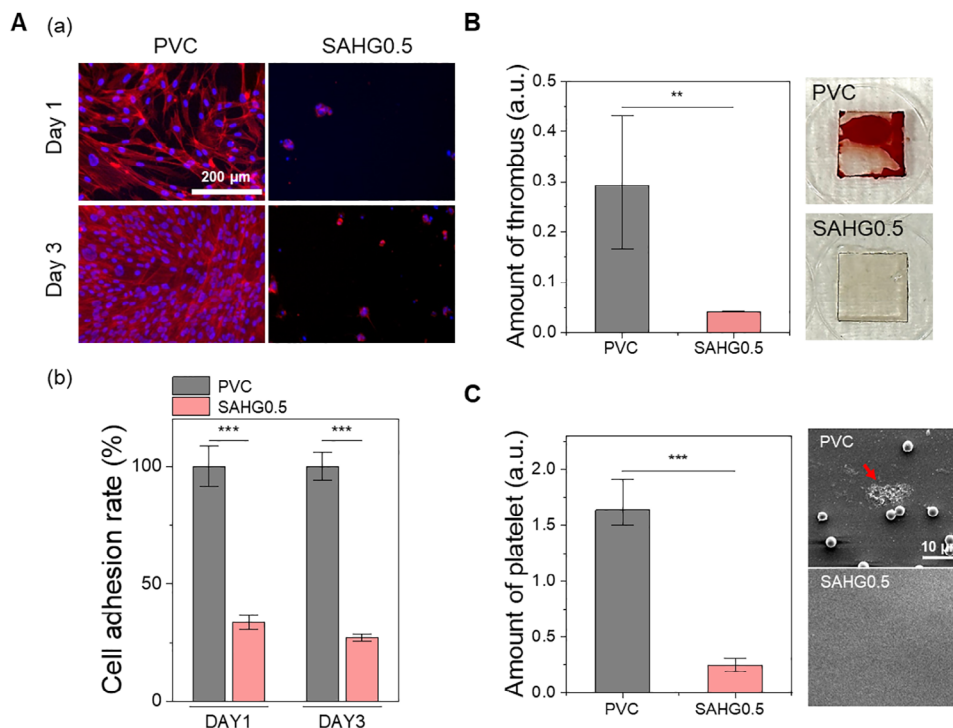


Figure 6. Antifouling and antithrombogenicity of SAHG0.5 coating. A) Cell morphology by Alexa Fluor 594-Phalloidin/DAPI staining (Red: F-actin, Blue: Nuclei) and adhesion rate of HDFs on the pristine PVC and SAHG0.5-coated PVC on day 1 and day 3. B) The relative amount of thrombus formed on the pristine PVC and SAHG0.5-coated PVC, and coagulated thrombus images on the surfaces. C) Quantification of adhering platelet activations on the pristine PVC and SAHG0.5-coated PVC and SEM images of each surface. $**p < 0.01$ and $***p < 0.001$.

trast, SAHG0.5 effectively inhibits both bacterial growth and attachment, demonstrating its superior bactericidal properties and highlighting its potential for advanced antibacterial applications.

It is widely accepted that bacterial biofilms contribute to over 80% of chronic infections, and *S. aureus* commonly exists in hospital environments. Particularly, preventing biofilm formation in advance is crucial because, once formed, biofilms are challenging to remove and resistant to immune responses in the human body.^[47] In our system, we anticipated that a thick hydration layer of pSBMA would inhibit the adherence of bacterial cell wall-anchored proteins, while the amine groups of pAEMA would subsequently work to kill all the barely attached bacteria, preventing biofilm formation. To evaluate the biofilm inhibitory ability, the SAHG0.5 surface and the other surfaces were exposed to the high-density droplet of *S. aureus* for 3 h and cultured in a fresh LB medium for 24 h. As seen in Figure 7B, the trend of biofilm formation decreased in the order of pristine PVC, SHG0.5, and SAHG0.5. Digital images revealed that the LB medium cultured with pristine PVC and SHG0.5 became blurry and opaque, indicating biofilm coverage. In the case of SHG0.5, a small number of bacteria that had not yet been removed seemed to proliferate and form biofilms, suggesting that a single antifouling effect is not sufficient to completely prevent biofilm formation. In contrast, the medium with SAHG0.5 remained clear and transparent, with no biofilm formation, due to the dual functionality of antifouling pSBMA hydrogel combined with bactericidal pAEMA. In the SEM images, additionally, circular shapes of *S. aureus* of the pristine PVC and SHG0.5 turned into star-shaped with bumpy surfaces in SAHG0.5, indicating positively charged amine groups

disrupted bacterial membranes to induce cell death. This anti-biofilm activity continued until day 14, demonstrating significant bactericidal effectiveness compared to SHG0.5 (Figure S11, Supporting Information).

2.8. Anti-Infective Activity of Dual-Functional p(SBMA-co-AEMA) Hydrogel In Vivo

To investigate the bactericidal effectiveness of SAHG0.5 in vivo, we constructed a subcutaneous bacterial infection model using Sprague Dawley (SD) rats. For the in vivo test, we chose titanium (Ti) as an implant substrate, which is well-known as one of the promising implantable biomaterials due to its good mechanical properties and biocompatibility.^[48] The pristine and hydrogel-coated Ti surfaces were exposed to *S. aureus* before the operation, and each infected sample was subcutaneously implanted under the backs of the rats. On days 1 and 3, all the substrates were collected, and the living bacteria on the surfaces were cultured on agar plates (Figure 8A). Compared to the pristine and SHG0.5, only the SAHG0.5-coated surface had almost no colonies on both days, indicating that the single antifouling effect of SHG0.5 alone was insufficient to prevent bacterial infections. In other words, the dual functionality of the SAHG0.5, which initially inhibits bacterial attachment and subsequently kills remaining bacteria on the surface, plays a key role in preventing infection aggravation.^[49] Furthermore, the histological images of the tissues in contact with the samples showed the recruitment of inflammatory cells (stained in dark purple) triggered by each sub-

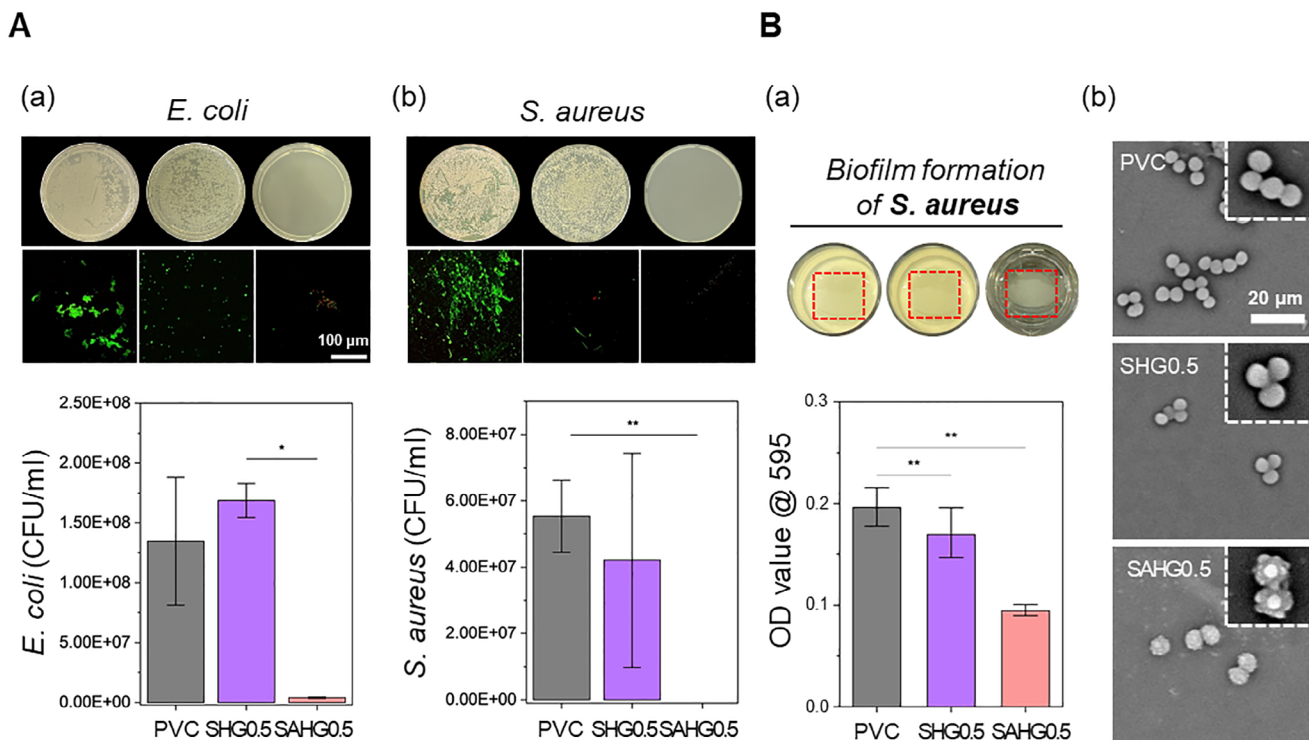


Figure 7. Bactericidal performance and biofilm inhibitory activity of SAHG0.5 coating. A) Representative colony (detached bacteria) and live-dead staining (attached bacteria, Green: live/ Red: dead) images of *E. coli* and *S. aureus* incubated on the pristine PVC, SHG0.5, and SAHG0.5-coated PVC. The number of bacteria detached was quantified using a colony counting method. B) Biofilm images formed on the pristine PVC, SHG0.5, SAHG0.5-coated PVC, and optical density (OD) values proportional to biofilm by crystal violet staining method. Representative SEM images of *S. aureus* on each sample. * $p < 0.05$ and ** $p < 0.01$.

strate (Figure 8B). A large number of inflammatory cells were observed in the pristine Ti and SHG0.5 groups, whereas a relatively negligible number of cells appeared around the SAHG0.5 surface. This demonstrated that the SAHG0.5 attacked only the bacteria without causing FBRs.

3. Conclusion

This study successfully developed a dual-functional p(SBMA-co-AEMA) hydrogel (SAHG0.5) surface by combining the zwitteri-

onic pSBMA with the cationic bactericidal pAEMA for biomedical applications. The hydrogel layer can be uniformly formed on various substrates, from metals to polymers, regardless of their geometry, via visible light cross-linking. To optimize the dual-functionality, we first adjusted the physical properties and antifouling performance of the zwitterionic SHG by varying the concentration of the cross-linker, pEGDMA. Subsequently, incorporating pAEMA into the hydrogel layer endowed it with bactericidal properties and reinforced the mechanical strength needed for a coating surface, decreasing the thick-

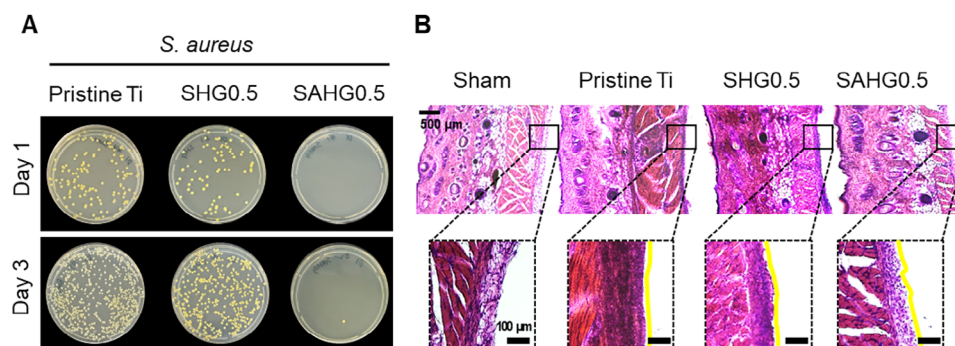


Figure 8. The anti-infective activity of SAHG0.5 coating in vivo. A) Photographs of *S. aureus* colonies on LB agar plates cultured from the pristine, SHG0.5, and SAHG0.5 coated Ti substrates after extraction. B) Representative H&E staining images of skin tissues around the implanted substrate on day 3 after the subcutaneous implantation. Enlarged images of each stained section are shown below, with the yellow lines indicating the areas directly in contact with the samples.

ness and swelling ratio. The optimized SAHG0.5 surface exhibited high biocompatibility and significant inhibitions of cells, platelets, and bacteria attachments. Importantly, the SAHG0.5 effectively prevented biofilm formation due to the contact-killing activity of amine groups, displaying long-term coating stability. These bactericidal performances were retained in vivo, as the SAHG0.5 coating substantially decreased bacterial growth in SD rats without inducing the foreign body response. Based on these results, we propose that this new coating method has great potential to prevent health-associated infections with its outstanding dual functionality and substrate-independent applicability.

4. Experimental Section

Materials: Unless otherwise noted, all chemicals were purchased from Sigma-Aldrich and used in as-received condition.

Preparation of SHG and SAHG Hydrogel Coating: All substrates were cleaned in isopropanol and deionized (DI) water under ultrasonication for 15 min and followed by drying with nitrogen. The substrates were then immersed in dopamine solution (2 mg mL⁻¹ in 10 mM Tris-HCl, pH8.5, BIOSESANG, Gyeonggi-do, Korea) and stirred at room temperature for 18 h. To immobilize photo-initiator on surface, Tris(2,2'-bipyridyl)dichlororuthenium(II) hexahydrate (Ru(bpy)₃) was reacted with synthesized silica nanoparticles (diameter 30 nm) in DI water overnight. After removing the solvent by centrifugation, Ru(bpy)₃-adsorbed SiO₂ nanoparticles were resuspended in 100% ethanol. Subsequently, [Ru(bpy)₃]²⁺/SiO₂ was immobilized on the pDA-coated substrates by a vertical deposition method, followed by washing and drying. For pSBMA and p(SBMA-co-AEMA) hydrogel coating, resultant substrates were immersed in each monomer solution and irradiated by visible light for 3 min, and the unreacted reagents were removed by dialysis against DI water for 24 h. More specific information about pre-gel solutions is described in Table 1.

Characterizations of the Hydrogel Coating Layer: The surface morphologies of hydrogel coating were analyzed by a scanning electron microscope equipped with energy-dispersive spectroscopy (SEM/EDS; Inspect F50, FEI, OR, USA) and an atomic force microscope (AFM; XE-100, Park Systems, Gyeonggi-do, Korea). The chemical compositions were confirmed by attenuated total reflection-Fourier transform infrared (ATR-FTIR; Nicolet iS20, Thermo Fisher Scientific, MA, USA), X-ray photoelectron spectroscopy (XPS; PHI 5000 VersaProbe, Ulvac-PHI, Kanagawa, Japan), and water contact angles (WCA) were analyzed by (SmartDrop, Femtobiomed, Gyeonggi-do, Korea). For measurement of hydrogel thicknesses, hydrogel-coated substrates were immersed in rhodamine B dye solution overnight to visualize the hydrogel layer on surfaces. After rinsing excess dye solution, the fluorescent images were obtained by an upright microscope (Eclipse Ts2R, Nikon, Tokyo, Japan) and analyzed using Image J software. Oscillatory rheological behavior of the hydrogels was evaluated using a rheometer (MCR102, Anton Paar, Graz, Austria) with frequency sweeps ranging from 0.1 to 100 Hz. Swelling behavior was evaluated using a gravimetric method. Each hydrogel was incubated in PBS for 1, 3, and 7 days at room temperature and freeze-dried when the weight reached equilibrium. The swelling ratio was calculated as follows.

$$\text{Swelling ratio (\%)} = \frac{M_w - M_d}{M_d} \times 100 \quad (1)$$

Mechanical Performance Evaluation of the Hydrogel Coating: To assess the mechanical robustness of the hydrogel coating, tape-peeling, compression, and adhesive strength tests were conducted. For the tape-peeling test, each sample surface was manually scratched with 1 mm spacing using a blade, followed by repeated application and removal of adhesive tape. Compressive and adhesive strengths were measured using an Instron universal testing machine (Model 5966, Instron Corp., MA, USA). For com-

pression testing, SHG0.5 and SAHG0.5 hydrogels were prepared as cylindrical samples (15 mm in diameter, 2 mm in height) and compressed at a crosshead speed of 5 mm min⁻¹ up to 95% strain. For adhesive strength measurements, each hydrogel sample was sandwiched between two rectangular substrates (PET, Ti, or SUS) and subjected to tensile loading at a rate of 1 mm min⁻¹ until interfacial fracture occurred. For time-dependent stability evaluation, SHG0.5- and SAHG0.5-coated PVC samples were immersed in PBS and incubated at 37 °C with shaking at 300 rpm for 72 h. Stability was assessed by measuring hydrogel thickness, water contact angle (WCA), and the amount of adsorbed BSA. For BSA adsorption tests, samples were exposed to 1% w/v BSA solution for 90 min, rinsed, and sonicated to remove loosely bound protein. Quantification was performed using the Bradford assay.

Cytotoxicity and Hemolysis Assay: To evaluate the cytotoxicity of the hydrogel-coated surfaces, HDFs were cultured in Dulbecco's modified Eagle's medium (DMEM; Gibco, Waltham, MA, USA) supplemented with 10% fetal bovine serum (FBS; Gibco) and 100 units mL⁻¹ of penicillin-streptomycin (Gibco) in a humidified atmosphere of 5% CO₂ at 37 °C. The pristine and the hydrogel-coated substrates were immersed in a cell culture medium for 24 h to obtain extraction. When the confluency of cells reached above 70% of a 75T flask, the cells were detached using Trypsin-EDTA (0.25%, 1X, Gibco) and seeded in a 24-well cell culture plate at a density of 5 × 10⁴ cells per well. After incubation overnight, the culture medium was replaced by substrate extractions and further incubated for 24 h. Finally, the cell viability was evaluated by CCK-8 and live-dead staining.

$$\text{Cell viability (\%)} = \frac{A_{\text{sample}} - A_{\text{blank}}}{A_{\text{control}} - A_{\text{blank}}} \times 100 \quad (2)$$

The hemolysis rate was investigated by incubating all the substrates with red blood cells (RBCs). To obtain the RBCs, the citrated whole sheep blood was centrifuged at 1200 rpm for 15 min and diluted 10 times with saline. Each sample was incubated in the diluted RBCs at 37 °C for 2 h and centrifuged at 1200 rpm for 15 min to acquire the supernatant. PBS and DI water were used as a negative and positive control, respectively. The absorbance was detected at 545 nm using a microplate reader (VersaMAX, Molecular Devices, CA, USA).

$$\text{Hemolysis (\%)} = \frac{A_{\text{sample}} - A_{\text{negative}}}{A_{\text{positive}} - A_{\text{negative}}} \times 100 \quad (3)$$

Cell Adhesion Test: To test the cell attachment on the pristine and each hydrogel-coated surface, HDFs (5 × 10⁴ cell mL⁻¹) were seeded on each surface (Square, 1 × 1 mm) and incubated for 1 and 3 days in a humidified atmosphere of 5% CO₂ at 37 °C. On the last day, adhering cells were fixed with 4% paraformaldehydes (Biosesang, Gyeonggi-do, Korea) for 20 min at room temperature and then permeabilized using 0.1% Triton-X 100 (Biosesang, Gyeonggi-do, Korea) in DPBS for 5 min. After blocked with 1% BSA for 30 min, the cells on each sample were stained with Alexa Fluor 594 Phalloidin (1:400, Thermo Fisher) for filamentous actin and 4'-6-diamidino-2-phenylindole (DAPI, 1:1000, Molecular Probes, OR, USA). Fluorescent images were acquired using fluorescent microscope and analyzed by Origin software (OriginLab Corporation, MA, USA).

Blood Clotting and Platelet Adhesion Test: Antithrombotic activities were investigated by exposing each sample to sheep blood (Kisan bio, Seoul, Korea). For the thrombus formation test, citrated sheep blood was pre-warmed in water bath and re-activated with 0.2 M calcium chloride and thrombin. The substrates were immersed in blood and incubated for 2 h at 37 °C, then washed with DI water. To quantify the amount of thrombus, the coagulated blood on the surfaces was broken down by ultrasonication for 30 min and the absorbance was measured at 545 nm using a microplate reader. Platelet activation was evaluated using PRP, which was isolated by centrifuging whole blood at 1500 rpm for 15 min and then re-activated in the same manner. After dropping PRP onto each surface and incubating it for 2 h at 37 °C, the adherent platelets were quantified by LDH assay kit (ab65393, abcam, United Kingdom) according to the manufacturer's

recommendations. To observe the morphology of the platelets, they were fixed with 2.5 wt.% glutaraldehyde solution and dehydrated in a series of ascending ethanol concentrations (50, 60, 70, 80, 90, and 100%).

Protein Adsorption Test: Quartz crystal microbalance with dissipation (QCM-D; Q-Sense Explorer, Biolin Scientific, Sweden) was used to compare the amount of protein adsorbed on the pristine and SHG0.5 coated surface. After establishing a baseline in PBS, BSA (10 mg mL⁻¹) and hFg (200 µg mL⁻¹) solution were injected at a 200 µL min⁻¹ flow rate for 15 and 60 min, respectively. Loosely adsorbed proteins were washed out by reinjecting PBS and variations in the frequency (ΔF) of each sample were analyzed using Qsoft401 software.

Bactericidal and Anti-Biofilm Test: The bactericidal activity was evaluated using *E. coli* (KCTC 2571) and *S. aureus* (KCTC 1621). Before the test, each bacterium was cultured in LB broth (BD Difco, NJ, USA) at 37 °C overnight to reach an exponential growth phase. The activated bacteria were diluted to 1 × 10⁸ CFU mL⁻¹. Subsequently, 20 µL of bacterial suspension was dropped on the pristine, SHG0.5, and SAHG0.5-coated PVC and incubated at 37 °C for 3 h. After then, loosely adhered bacteria washed out by PBS and were spread onto LB agar (BD Difco, NJ, USA) plates and quantified with a colony counting method. The remaining bacteria were visualized by a live-dead staining using BacLight bacterial viability kit (Invitrogen, OR, USA) according to the manufacturer's instructions. For the biofilm formation, *S. aureus* adhered on the surfaces were transferred to the fresh LB broth and cultured at 37 °C overnight. The biofilm formed on the culture plate was quantitatively measured by crystal violet staining and the morphologies of *S. aureus* were observed after fixed with 2.5 wt.% glutaraldehyde solution and dehydrated in a series of ascending ethanol concentrations (50, 60, 70, 80, 90, and 100%).

In Vivo Anti-Infective Test: All animal-related procedures were performed with the approval of the Institutional Animal Care and Use Committee (IACUC) (Protocol No. KIST-IACUC-2022-014-5). The experimental sections were divided into 4 groups: Sham, Pristine Ti, SHG0.5-coated Ti, and SAHG0.5-coated Ti. The substrates are cut into a round shape with a diameter of 1 cm and sterilized. Before the implantation, all samples were treated with 20 µL of *S. aureus* (1 × 10⁸ CFU mL⁻¹ in PBS) and incubated at 37 °C for 1 h. The male SD rats (7 W, DBL, Chungbuk, Korea) of 170–220 g were respiratorily anesthetized by isoflurane and shaved. Subsequently, the pre-infected substrates with *S. aureus* were implanted into the incisions of rats. After 1 and 3 days, the substrates were collected, and surrounding tissues were harvested from the humanly euthanized rats. The bacteria on the surfaces were detached in PBS by ultrasonication and cultured in LB agar plates for 48 h. The harvested tissues were fixed in 10% formalin, dehydrated, and embedded in a frozen section solution (Leica, Germany). The frozen samples were cut into small slices, stained with H&E staining and observed by a light microscope.

Statistical Analysis: The quantitative data are expressed as the mean ± standard error of the mean (SEM). Statistical analysis was performed using one-way ANOVA and two-sample t-tests with Origin software (Origin-Lab Corporation, USA). Significance levels are represented as follows: * for p < 0.05, ** for p < 0.01, *** for p < 0.001. These significance levels are indicated in each figure. All experiments were conducted at least three times (n ≥ 3), unless stated otherwise.

Supporting Information

Supporting Information is available from the Wiley Online Library or from the author.

Acknowledgements

This research was financially supported by the Nano Material Technology Development Program (2021M3H4A1A04092879) and the National R&D Program (RS-2023-00211412) through the National Research Foundation (NRF) of Korea funded by the Ministry of Science and ICT. This work was also supported by the KIST Research Program (2E33151, 2E3312L, 2E33148, and 2E33145).

Conflict of Interest

The authors declare no conflict of interest.

Data Availability Statement

The data that support the findings of this study are available from the corresponding author upon reasonable request.

Keywords

antifouling, antithrombogenic, bactericidal, surface coatings, zwitterionic hydrogels

Received: July 12, 2024

Revised: April 25, 2025

Published online:

- [1] M. Fu, Y. Liang, X. Lv, C. Li, Y. Y. Yang, P. Yuan, X. Ding, *J. Mater. Sci. Technol.* **2021**, *85*, 169.
- [2] T. Egghe, R. Morent, R. Hoogenboom, N. De Geyter, *Trends Biotechnol.* **2023**, *41*, 63.
- [3] S. Roh, Y. Jang, J. Yoo, H. Seong, *BioChip J.* **2023**, *17*, 174.
- [4] V. B. Damodaran, N. S. Murthy, *Biomater. Res.* **2016**, *20*, 18.
- [5] J. S. Kumar, R. Kumar, R. Verma, *Acta Metall. Sin. (Engl. Lett.)* **2024**, *37*, 213.
- [6] D. Chan, J.-C. Chien, E. Axpe, L. Blankemeier, S. W. Baker, S. Swaminathan, V. A. Piunova, D. Y. Zubarev, C. L. Maikawa, A. K. Grosskopf, J. L. Mann, H. T. Soh, E. A. Appel, *Adv. Mater.* **2022**, *34*, 2109764.
- [7] J. Yoo, A. Birke, J. Kim, Y. Jang, S. Y. Song, S. Ryu, B.-S. Kim, B.-G. Kim, M. Barz, K. Char, *Biomacromolecules* **2018**, *19*, 1602.
- [8] J. Lee, J. Yoo, J. Kim, Y. Jang, K. Shin, E. Ha, S. Ryu, B.-G. Kim, S. Wooh, K. Char, *ACS Appl. Mater. Interfaces* **2019**, *11*, 6550.
- [9] S. Y. Jang, S. Roh, K. Seo, Y. Jung, H. Y. N. Thi, J. F. Kim, H. An, H. Jeon, I. K. Kwon, J. Yoo, *Carbohydr. Polym.* **2025**, *348*, 122875.
- [10] Y. Jang, S. Roh, Y. Cho, Y. Jung, K. Lee, N. Choi, J. Yoo, H. Seong, *Adv. Fiber Mater.* **2024**, *6*, 1583.
- [11] L.-Y. Zhang, D.-Q. Feng, P.-Y. Zhu, W.-L. Song, M. Yasir, C. Zhang, L. Liu, *ACS Appl. Mater. Interfaces* **2023**, *15*, 13644.
- [12] T. Peng, Q. Shi, M. Chen, W. Yu, T. Yang, *J. Funct. Biomater.* **2023**, *14*, 243.
- [13] Y. Yu, H. Yuk, G. A. Parada, Y. Wu, X. Liu, C. S. Nabzdyk, K. Youcef-Toumi, J. Zang, X. Zhao, *Adv. Mater.* **2019**, *31*, 1807101.
- [14] M. Gori, S. M. Giannitelli, G. Vadalà, R. Papalia, L. Zollo, M. Sanchez, M. Trombetta, A. Rainer, G. Di Pino, V. Denaro, *Molecules* **2022**, *27*, 3126.
- [15] M. Yao, H. Sun, Z. Guo, X. Sun, Q. Yu, X. Wu, C. Yu, H. Zhang, F. Yao, J. Li, *Chem. Eng. J.* **2021**, *421*, 129702.
- [16] V.-S. Luc, C.-C. Lin, S.-Y. Wang, H.-P. Lin, B.-R. Li, Y.-N. Chou, C.-C. Chang, *Biomacromolecules* **2023**, *24*, 5467.
- [17] M. Kobus, T. Friedrich, E. Zorn, N. Burmeister, W. Maison, *J. Med. Chem.* **2024**, *67*, 5168.
- [18] D. Karagrigoriou, B. B. Berking, Q. Wang, D. M. Sánchez-Cerrillo, D. R. Galimberti, D. A. Wilson, K. Neumann, *ACS Macro Lett.* **2023**, *12*, 1608.
- [19] B. B. Berking, G. Poulladonou, D. Karagrigoriou, D. A. Wilson, K. Neumann, *Angew. Chem. Int. Ed. Engl.* **2023**, *62*, 202308971.
- [20] N. Erathodiyil, H.-M. Chan, H. Wu, J. Y. Ying, *Mater. Today* **2020**, *38*, 84.
- [21] T. Xiang, C.-D. Luo, R. Wang, Z.-Y. Han, S.-D. Sun, C.-S. Zhao, *J. Membr. Sci.* **2015**, *476*, 234.

- [22] Q. Yu, Z. Wu, H. Chen, *Acta Biomater.* **2015**, *16*, 1.
- [23] L. C. Paslay, B. A. Abel, T. D. Brown, V. Koul, V. Choudhary, C. L. McCormick, S. E. Morgan, *Biomacromolecules* **2012**, *13*, 2472.
- [24] M. Yao, Z. Wei, J. Li, Z. Guo, Z. Yan, X. Sun, Q. Yu, X. Wu, C. Yu, F. Yao, S. Feng, H. Zhang, J. Li, *Nat. Commun.* **2022**, *13*, 5339.
- [25] E. J. Walker, Jr., C. K. Pandiyarajan, K. Efimenko, J. Genzer, *ACS Appl. Polym. Mater.* **2019**, *1*, 3323.
- [26] L. Chen, L. Tan, S. Liu, L. Bai, Y. Wang, *J. Biomater. Sci.* **2014**, *25*, 766.
- [27] J. Shen, M. Du, Z. Wu, Y. Song, Q. Zheng, *RSC Adv.* **2019**, *9*, 2081.
- [28] B. Tambosco, K. Segura, C. Seyrig, D. Cabrera, M. Port, C. Ferroud, Z. Amara, *ACS Catal.* **2018**, *8*, 4383.
- [29] K. S. Lim, B. J. Klotz, G. C. J. Lindberg, F. P. W. Melchels, G. J. Hooper, J. Malda, D. Gawlitta, T. B. F. Woodfield, *Macromol. Biosci.* **2019**, *19*, 1900098.
- [30] F. Haryanto, A. Mahardian, *IOP Conf. Ser.: Mater. Sci. Eng.* **2018**, *288*, 012076.
- [31] J. Zhang, M. Wu, P. Peng, J. Liu, J. Lu, S. Qian, J. Feng, *ACS Appl. Mater. Interfaces* **2022**, *14*, 56097.
- [32] M. L. Hair, *J. Non-Cryst. Solids* **1975**, *19*, 299.
- [33] C. Cha, E. Antoniadou, M. Lee, J. H. Jeong, W. W. Ahmed, T. A. Saif, S. A. Boppart, H. Kong, *Angew. Chem., Int. Ed.* **2013**, *52*, 6949.
- [34] N. A. Peppas, A. R. Khare, *Adv. Drug Delivery Rev.* **1993**, *11*, 1.
- [35] T. Ekblad, G. Bergström, T. Ederth, S. L. Conlan, R. Mutton, A. S. Clare, S. Wang, Y. Liu, Q. Zhao, F. D'Souza, G. T. Donnelly, P. R. Willemsen, M. E. Pettitt, M. E. Callow, J. A. Callow, B. Liedberg, *Biomacromolecules* **2008**, *9*, 2775.
- [36] M. He, K. Gao, L. Zhou, Z. Jiao, M. Wu, J. Cao, X. You, Z. Cai, Y. Su, Z. Jiang, *Acta Biomater.* **2016**, *40*, 142.
- [37] J. Fatisson, S. Mansouri, D. Yacoub, Y. Merhi, M. Tabrizian, *J. R. Soc. Interface* **2011**, *8*, 988.
- [38] Y. Qiu, A. C. Brown, D. R. Myers, Y. Sakurai, R. G. Mannino, R. Tran, B. Ahn, E. T. Hardy, M. F. Kee, S. Kumar, G. Bao, T. H. Barker, W. A. Lam, *Proc. Natl. Acad. Sci. USA* **2014**, *111*, 14430.
- [39] L. Wei, J. Huang, Y. Yan, J. Cui, Y. Zhao, F. Bai, J. Liu, X. Wu, X. Zhang, M. Du, *ACS Appl. Polym. Mater.* **2022**, *4*, 4876.
- [40] Y. B. Lee, Y. M. Shin, J.-h. Lee, I. Jun, J. K. Kang, J.-C. Park, H. Shin, *Biomaterials* **2012**, *33*, 8343.
- [41] S. E. Exley, L. C. Paslay, G. S. Sahukhal, B. A. Abel, T. D. Brown, C. L. McCormick, S. Heinhorst, V. Koul, V. Choudhary, M. O. Elasmri, S. E. Morgan, *Biomacromolecules* **2015**, *16*, 3845.
- [42] L. Bonda, J. Müller, L. Fischer, M. Löwe, A. Kedrov, S. Schmidt, L. Hartmann, *Polymers* **2023**, *15*, 3663.
- [43] B. D. Ratner, *Biomaterials Science: An Introduction to Materials in Medicine*, Academic press, San Diego **2004**.
- [44] M. Wancura, A. Nkansah, A. Robinson, S. Toubbeh, M. Talanker, S. Jones, E. Cosgriff-Hernandez, *Ann. Biomed. Eng.* **2024**, *52*, 1804.
- [45] G. Parada, Y. Yu, W. Riley, S. Lojovich, D. Tshikudi, Q. Ling, Y. Zhang, J. Wang, L. Ling, Y. Yang, S. Nadkarni, C. Nabzdyk, X. Zhao, *Adv. Healthcare Mater.* **2020**, *9*, 2001116.
- [46] A. J. Chu, *Int. J. Inflamm.* **2011**, *2011*, 367284.
- [47] Q. Peng, X. Tang, W. Dong, N. Sun, W. Yuan, *Antibiotics* **2023**, *12*, 12.
- [48] F. Yang, D. Huo, J. Zhang, T. Lin, J. Zhang, S. Tan, L. Yang, *J. Colloid Interface Sci.* **2023**, *638*, 1.
- [49] H. Mitwalli, R. Alsahafi, A. A. Balhaddad, M. D. Weir, H. H. K. Xu, M. A. S. Melo, *Bioengineering* **2020**, *7*, 83.